ChemPubSoc Europe

DOI: 10.1002/celc.201800603

CHEMELECTROCHEM Articles

High Performance N-Doped Carbon Electrodes Obtained via Hydrothermal Carbonization of Macroalgae for Supercapacitor Applications

Meng Ren,[a] Ziyang Jia,[a] Zhongwei Tian,[a] Diana Lopez,[b] Jinjun Cai,*[a, c] Maria-Magdalena Titirici,*[c] and A. Belen Jorge*[c]

The conversion of bio-waste into useful porous carbons constitutes a very attractive approach to contribute to the development of sustainable energy economy, even more as they can be used in energy storage devices. Here we report the synthesis of N-doped carbons from hydrothermal carbonization of macroalgae, *Enteromorpha prolifera (EP)*, followed by a mild KOH activation step. The obtained N-doped carbons exhibited surface areas of up to ~2000 m^2/g with N-loadings varied in the range of 1.4~2.9 at%. By modifying activation temperature, we were able to tune the surface chemistry and porosity, achieving excellent control of their properties. The specific capacitance reached values of up to 200 F/g at 1 A/g in 6 M KOH for the sample obtained at activation temperature of 700 °C (AHC-*700*). The symmetric supercapacitor using the sample activated at 800 °C (AHC-*800*) as electrodes exhibited the highest cycling stability of the samples studied in this work, with capacitance retention of up to 96% at 10 A/g, even after 10,000 cycles, constituting the highest reported for biomass-derived carbon electrodes. These results show the great potential of N-doped carbons as electrodes for supercapacitors and confirm the excellent electrochemical properties of biomass-derived carbons in energy storage technologies.

1. Introduction

N-doped porous carbons have attracted great interest due to their improved performance as electrodes in electrochemical storage, compared to their un-doped analogous.[1–6] However, the synthesis of N-doped carbons usually requires long steps, which involve high carbonization temperature and further post-treatment to introduce N. They can also be obtained from direct pyrolysis of N-enriched metal-organic frameworks (MOFs)[7,8] and polymers such as the polypyrrole, polydopamine or polyacrylonitrile.[9–11] However, organic precursors are less available than biomass.[12–16] Biomass-derived N-doped carbons have been recently prepared from hydrothermal pyrolysis and activation processes.[2,17,18] Sevilla et al.[13] reported N-doped carbons with surface areas of ~2400 m^2/g from hydrothermal carbonization and activation using microalgae as biomass precursor. The use of biomass-derived cellulose for producing porous carbons as electrodes for supercapacitor has also been reported giving excellent performance[19] and the incorporation of certain types heteroatoms into frameworks has shown to notably increase the energy storage capacity.[4,6,20] Moreover, freestanding biomass-derived have also been recently developed as potential candidates for flexible energy storage devices.[21]

Algae biomass is known to exhibit remarkable photosynthetic efficiency and fast growth rate. It mainly consists of lipids, carbohydrates, proteins, and nucleic acid, all of which is excellent precursor for carbon materials.[16,22] Gu et al.[23] reported carbons from cyanobacteria pyrolysis with surface area of 2184 m^2/g, showing a specific capacitance of 222 F/g at 5 A/g in 6 M KOH. Several studies reported the hydrothermal synthesis of microalgae-derived N-doped carbons,[12,13,15,24,25] exhibiting remarkable electrochemical storage performance, attributed to both their high porosity and to the N-species inherent from the high protein fraction present in microalgae. Macroalgae, an important member of the marine biomass, has also been reported to possess interesting energy storage properties. Beguin et al.[26] produced hierarchical porous carbons from pyrolysis of the macroalgae *Lessonia Nigrescens*, showing high capacitance in acid electrolyte. N-doped carbons from carbonization of *Undaria pinnatifida* with surface area of 1200 m^2/g also exhibited great potential as metal-free electrocatalyst for oxygen reduction reaction in fuel cells.[27] Unlike microalgae, there are only few reports describing N-doped carbons derived from macroalgae biomass, especially from hydrothermal treatment.[28,29] We believe that macroalgae is an

[a] *M. Ren, Z. Jia, Z. Tian, Dr. J. Cai*
School of Chemical Engineering
Xiangtan University
Xiangtan 411105, China
E-mail: caijj@xtu.edu.cn
[b] *Prof. D. Lopez*
Institute of Chemistry
University of Antioquia
A.A. 1226, Medellín, Colombia
[c] *Dr. J. Cai, Prof. Dr. M.-M. Titirici, Dr. A. B. Jorge*
School of Engineering Materials & Science
Queen Mary University of London
London, E1 4NS, UK
E-mail: a.sobrido@qmul.ac.uk
m.m.titirici@qmul.ac.uk
j.cai@qmul.ac.uk

Supporting information for this article is available on the WWW under https://doi.org/10.1002/celc.201800603

abundant sustainable source of C,N-based materials that can potentially lead to highly efficient nanostructured electrodes for energy storage applications.

Enteromorpha prolifera (EP) is a marine macroalgae which has rapidly grown due to warmer climate and eutrophication. This has led to a large-scale of *EP* gathered off the coasts of China every year.[30–33] The conversion of *EP* into functional carbons that can be used as electrode materials in supercapacitors constitutes a convenient choice that could help solve this environmental problem. We reported N-doped hierarchical carbons from direct carbonization of *EP* algae with surface area of 422 m^2/g.[30] Lately, several studies have also reported *EP*-based carbons with surface areas up to 3330 m^2/g obtained through conventional carbonization, followed by KOH chemical activation for electrochemical storage applications,[3,32–36] confirming that *EP* would be a good choice as raw material for N-doped carbons. Very recently, Wang et al.[37] reported *EP*-based carbons from the one-step KOH activation method as electrodes for sodium-ion capacitors, exhibiting high-energy density of ~84 Wh/kg. All the above-mentioned results indicate that *EP* algae is a promising low-cost precursor for high-performance carbon electrodes for energy storage applications. However, to the best of our knowledge, no reports about *EP*-based carbons produced from hydrothermal carbonization have been published. Here we present the preparation of electroactive N-doped carbons via hydrothermal treatment of *EP* macroalgae exhibiting excellent structural and chemical features which make them ideal candidates as electrodes in supercapacitors. Significantly, the symmetric supercapacitors prepared with these N-doped carbons showed remarkable capacitance retention, of up to 96%, even at 10 A/g current density, in 6 M KOH electrolyte. The results suggest that the prepared N-doped carbons are excellent electrode materials for supercapacitors with high rate stability and performance.

2. Results and Discussion

The thermal behaviour of both dried *EP* algae and *EP* hydrothermally treated at 180 °C (hydrothermal *EP* algae) was studied by thermogravimetric analysis (TGA). The data showed four loss stages as shown in Figure 1. There is an initial loss (stage I) observed for both samples, occurring below 100 °C attributed to evaporation of adsorbed moisture.[26] Stage II (100–400 °C) shows significant differences for both *EP* materials. Dried algae undergo a sharp loss of weight starting at around 250 °C, associated with the removal of residual water in *EP* cells,[31] while hydrothermal *EP* does not start losing weight until temperature reaches 350 °C. As it can be clearly observed from Figure 1, both materials have lost ~40% weight at 400 °C, indicating the decomposition of carbohydrates, proteins and cellulose, and constitutes the main pyrolysis stage. From 400 to 600 °C (stage III), both samples undergo little change. During stage IV (600 to 800 °C) graphitization and elimination of N,O-species and unstable C atoms take place. During this stage, the hydrothermal *EP* suffered almost no further weight loss with only graphitization taking place up to 800 °C, whereas the

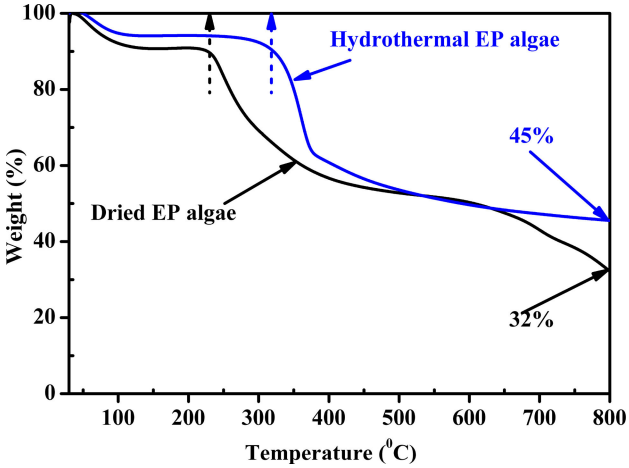

Figure 1. TGA of dried *EP* algae and hydrothermal treated *EP* algae under N_2 flow from room temperature to 800 °C.

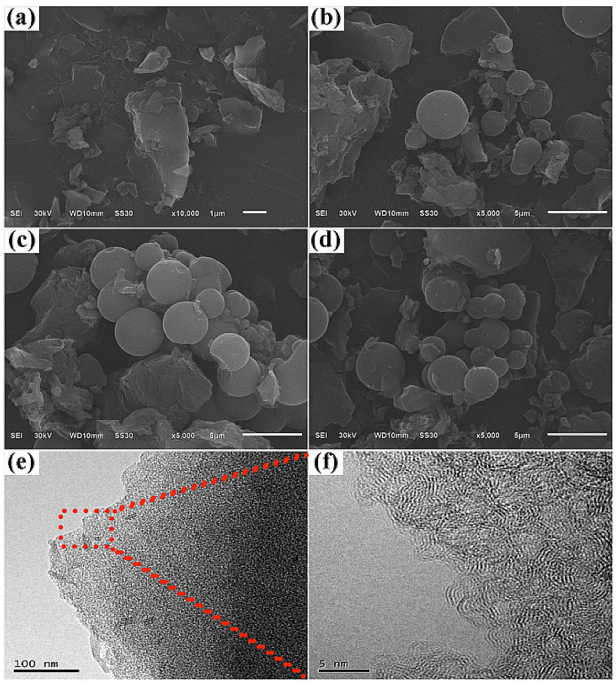

Figure 2. SEM images of a) hydrochars prepared at 450 °C; hydrothermal carbons (AHC-y) prepared at b) 600 °C (AHC-*600*), c) 700 °C (AHC-*700*), and (d) 800 °C (AHC-*800*). e), f) HRTEM images for AHC-*800*.

weight loss of dried *EP* is significant, with a remaining weight of ~32%. The TGA experiments confirmed the higher stability of the carbon obtained by hydrothermal carbonization, with respect to the conventional carbonization approach.

The morphology of the hydrochar and N-doped carbons was studied using scanning-electron microscopy (SEM) and transmission electron microscopy (TEM) techniques (Figure 2), revealing an interesting change from hydrochar to N-doped carbons. As shown in Figure 2a, hydrochars consisted of mainly bulk structure with irregular particles morphology, while particles with spherical shape were observed for the hydrothermal N-doped carbons (Figure 2b, c, d). Microsphere-shaped

carbon particles obtained by hydrothermal co-carbonization of microalgae (*S. Platensis*) and glucose have also been reported by Sevilla et al.[12] This finding also matched with microspheres widely described in literature when glucose or sucrose are used as only raw materials.[14] The formation of particles with spherical morphology was previously reported by Wu et al.[38] when treating starch under hydrothermal conditions with no glucose or sucrose addition. This result suggests hydrothermal conditions promote the occurrence of spherical particles, as this effect is not observed when the conventional carbonization route is employed and no glucose or sucrose are added. The irregular shaped particles also observed by SEM, are common in carbons produced from biomass materials. SEM images showed that thermal treatment at higher temperature promoted further transformation of the carbohydrates present in the *EP* (Figure 2b, c, d).[17,29] The TEM images corresponding to the hydrothermal carbon treated at the highest temperature (800 °C), AHC-*800* (Figure 2e, f) confirmed the formation of micropores, which are expected to contribute positively to the performance of the material as electrode for supercapacitors.[26]

The x-ray diffraction patterns (XRD) of the hydrothermal N-doped carbons AHC-*y* (where *y* represents the activation temperature) (Figure S1a) exhibited two broad very weak bands at 23 and 44° 2θ. These corresponded to the (002) and (100) reflections, typically observed in carbons.[30,39] However, the low intensity and broadness of the two peaks indicated a low degree of graphitization for the carbons produced. The peak appearing at around 18° observed in the x-ray diffraction pattern of the AHC-*600* corresponds to residual inorganic component of the algae, as previously described by Yue et al.[35]. At higher temperatures, this inorganic fraction decomposes and no x-ray diffraction peak at 18° is longer observed. Raman spectroscopy results confirmed the low degree of graphitization of samples (Figure S1). All the spectra exhibited two bands at around 1598 and 1347 cm^{-1} from the G- and D-bands, respectively, commonly present in carbons.[30] The ratio between relative intensity of D-band and G-band (I_D/I_G) was used to assess the degree of graphitization of the samples,[40,41] with the smaller ratio meaning higher degree of ordering. The calculated I_D/I_G data based on the Gaussian deconvolution are found to be about 0.85, 1.58 and 1.11 for AHC-*600*, AHC-*700* and AHC-*800*, respectively. The higher activation temperature of 800 °C resulted, as expected, in higher graphitization for AHC-*800*. The low value I_D/I_G for AHC-*600* should not be taken into account, as this is due to the presence of inorganic compounds in algae (Figure S1a).

The N_2 sorption isotherms and corresponding pore size distributions (PSDs) for the AHC-*y* samples are illustrated in Figure 3, with the detailed parameters summarized in Table 1. The N_2 isotherms exhibited a typical behaviour for a microporous material (Figure 3a). The absence of hysteresis loop in the isotherms indicated high percentage of micropores with small fraction of mesopores.[39,42] AHC-*600* showed the highest ratio of micropores, but the lowest surface area, of 952 m^2/g (Figure 3a). Increasing the activation temperature can increase significantly the adsorbed N_2, leading to an enlargement of surface area and pore volume. The calculated Brunauer-Emmett-Teller (BET) surface area and pore volume for AHC-*700* were of 1528 m^2/g and 0.66 cm^3/g, respectively, and up to 1979 m^2/g and 0.85 cm^3/g in the case of AHC-*800* (Table 1). The microporosity of N-doped porous carbons decreased with an increasing carbonization temperature, from 91.1% to 82.3% (Table 1), evidencing that the severer activation conditions widen small-sized micropores to form large-sized micropores or small-sized mesopores with breakage between adjacent micropores. PSDs indicated homogeneous microporosity, with pore sizes of ~3.0 nm (Figure 3b). The activation treatment at higher temperature favoured the formation of small-sized mesopores,

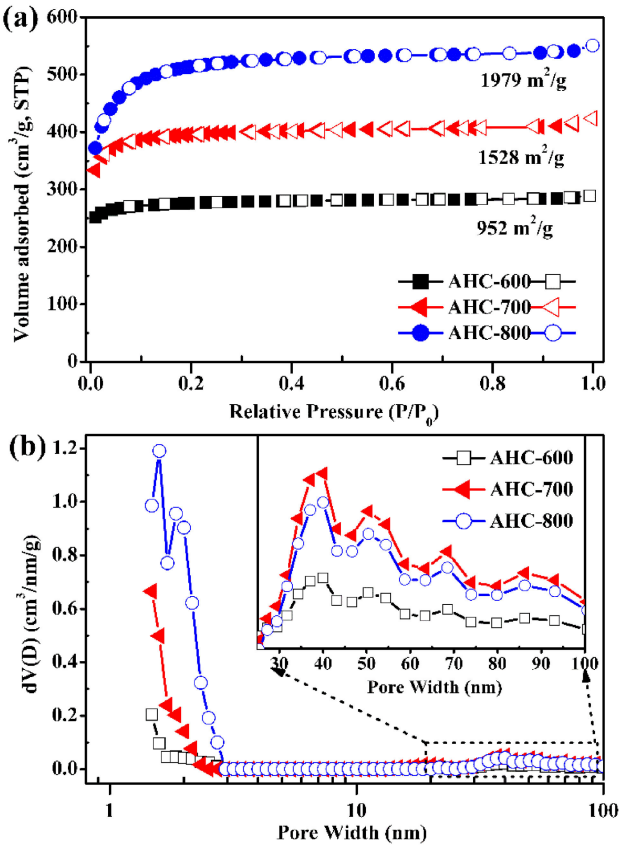

Figure 3. a) The N_2 adsorption-desorption isotherms of AHC-*y* carbons and b) the corresponding PSDs calculated from adsorption branch of N_2 isotherms using DFT model.

Table 1. Pore texture from N_2 adsorption and surface-doping chemistry of AHC-*y* carbons.

Samples	S_{BET} [m^2/g][a]	V_{total} [cm^3/g][b]	R [%][c]	D_p [nm][d]	XPS analysis [at%] C	N	O
AHC-600	952 (844)	0.45 (0.41)	91.1	1.88	85.86	2.89	11.25
AHC-700	1528 (1337)	0.66 (0.58)	87.8	1.71	88.55	2.4	9.05
AHC-800	1979 (1451)	0.85 (0.70)	82.3	1.72	90.36	1.4	8.24

[a] BET surface area and data in parentheses are micropore surface areas; [b] Total pore volume and data in parentheses are micropore volumes; [c] Microporosity determined from data of V_{micro} divided by V_{total}; [d] Average pore size determined from Dubinin-Astakhov (DA) method.

leading to an increase of surface area and pore volume (Figure 3b). As shown in the inset of Figure 3b, the amount of large-sized mesopores is higher for AHC-*700* and AHC-*800,* compared to AHC-*600*, which is expected to be beneficial for capacitive performance, especially at high current densities.[37] The goodness of BET surface area calculations is illustrated in Figure S2. The high degree of linearity, with coefficients up to 0.999, indicated the relative pressure (P/P_0) in the 0.02–0.10 range for calculating surface areas is realistic.

The elemental content at the surface of the AHC-*y* carbons was determined by XPS. The XPS survey spectrum of AHC-*600* is presented in Figure S3, showing three predominant peaks that correspond to C1s, N1s, and O1s at around 285, 400, and 532 eV, respectively. High-resolution C1s, N1s, and O1s XPS spectra for the prepared N-doped carbons are shown in Figure 4 and Figure S4. Four binding environments with binding energies at around 398.5, 400.4, 401.3, and 403.3 eV were found, ascribed to pyridinic, pyrrolic, graphitic and pyridine-N-oxide, respectively (Figure 4).[1,43] High-resolution C1s and O1s XPS spectra for all carbons demonstrating the existence of C and O atoms with different coordination environments are presented in Figure S4. High resolution C1s XPS spectra were very similar for all AHC-*y*. They exhibited four peaks at around 284.6, 285.2, 286.2, and 288.4 eV, attributed to C=C, C–N, C=N/C=O, and O-C=O functional groups, respectively [32,43] (Figure S4a). The high-resolution O1s spectra in Figure S4b, c, d can be deconvoluted into three peaks at around 531.8, 532.5, and 533.3 eV, assigned to C=O, C–O, and C–OH groups, respectively.[23,32] As it can be seen from Table 1, O and N content decreased with increasing of activation temperature. The highest N content corresponded to AHC-*600*, of about 2.9 at.% (Table 1), lower than that found in the sample prepared via direct carbonization with N content of 4.22 at %,[32] indicating that activation step partially consumed N-groups in precursors. The proportions (%) of various N- and O-species in relationship to their functionalities are shown in Figure 5. The pyrrolic N was dominant in all carbons, with the highest ratio in the case of AHC-*600*. The content of graphitic N-oxide was notably higher in the case of AHC-*700* and AHC-*800*, implying that pyridinic N is not stable at high temperature, and is partially transformed to graphitic N and pyridine-N-oxide.

The electrochemical storage properties of AHC-*y* N-doped carbons for supercapacitor applications were explored. Cyclic voltammogram (CV) curves of all AHC-*y* N-doped C based supercapacitors (Figure 6a) exhibited a semi-rectangular shape, indicating main double layer capacitance and limited pseudo-capacitance, due to the existence of N, O-based functional groups. A slight distortion of rectangular shape was observed

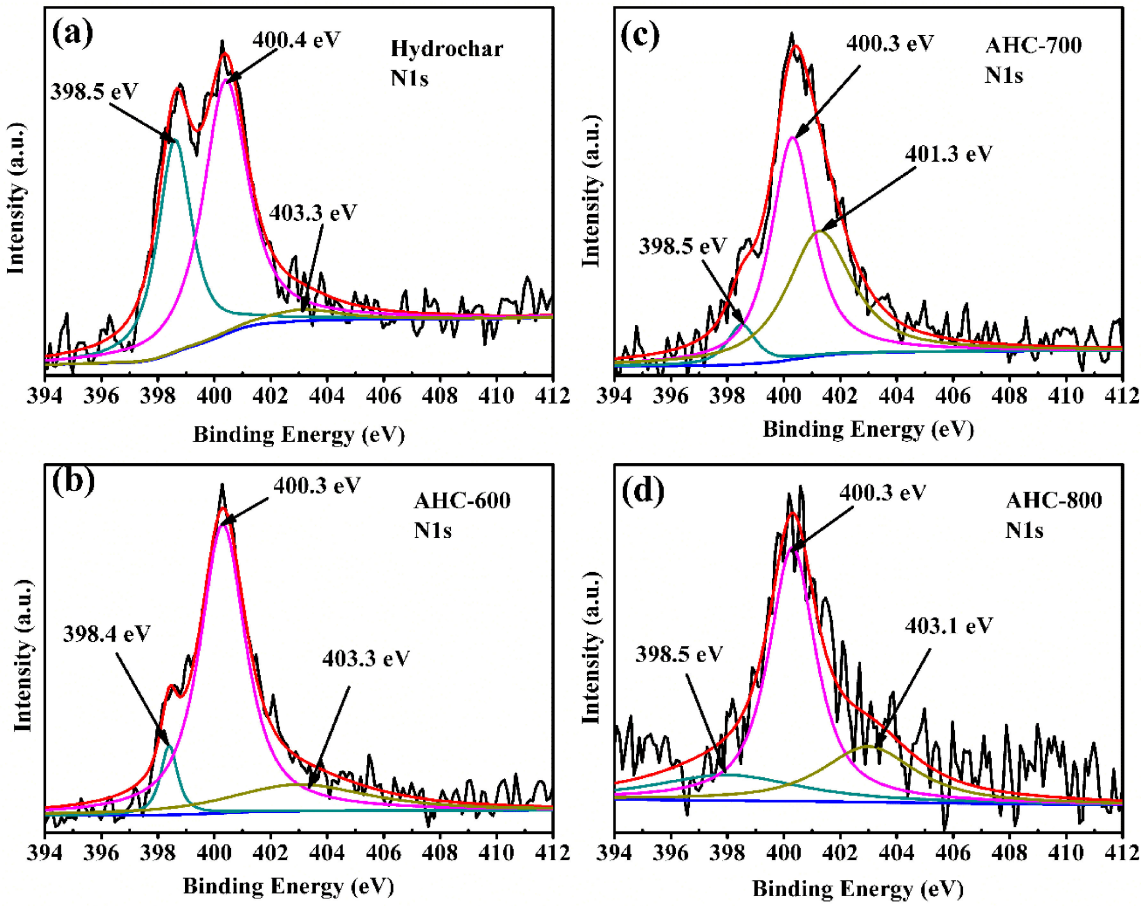

Figure 4. High-resolution N1s line XPS spectra of a) Hydrochar prepared at 450 °C, b) AHC-*600*, c) AHC-*700*, and d) AHC-*800*.

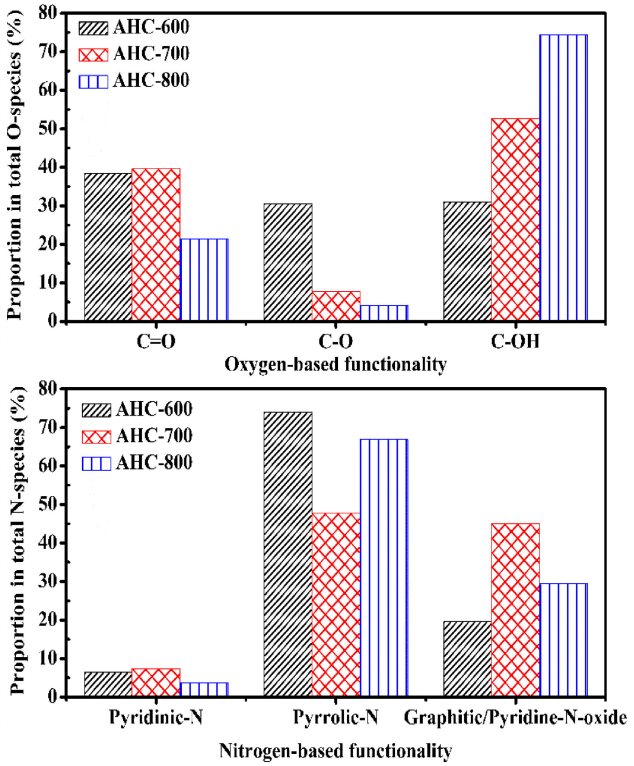

Figure 5. Proportions (%) of various O and N-based functionality in the total O and N functional groups for the AHC-*y* carbons.

for the CV curve of AHC-*600*-based supercapacitor (Figure 6a). AHC-*700*-based supercapacitor showed the largest capacitance and longest discharge time (Figure 6b). Specific capacitances of 178, 200, and 184 F/g at 0.5 A/g current density were obtained for AHC-*600*, AHC-*700*, and AHC-*800*, respectively. The capacitance value is remarkably affected by both the surface area and surface-elemental content. In general, the N-doped carbons with larger surface area should have higher specific capacitance.[24] However, AHC-*700* exhibited the largest capacitance (whereas AHC-*800* has the higher surface area) (Table 1). We believe that the higher content of graphitic N-species in AHC-*700* has an important effect in the greater capacity value, due to the existing pseudo-capacitance, which could be confirmed from the redox peaks of CV curve in the 0.1–0.3 V range (Figure 6a). The current response increased with increasing the scan rate (Figure 6c). The CV curves for AHC-*800*-based supercapacitors remained semi-rectangular shape even at 300 mV/s scan rate (Figure S5), indicating its superior high rate capacitive behaviour, which is attributed to its existing small-sized mesopores in the range of 2.0–3.0 nm. All galvanostatic charge/discharge (GCD) curves showed highly linear behaviour and nearly symmetric triangular properties (Figure 6d, Figure S5). Only a small voltage drop (*IR*) was observed at 10 A/g current density with *IR* values of ~0.08, 0.07, and 0.05 V for AHC-*600*, AHC-*700*, and AHC-*800*, respectively, indicating excellent coulombic efficiency for all samples.[20,44] The specific capacitance at various current densities were plotted in Figure 6e, with capacitance values of 198, 228, and 214 F/g at 0.1 A/g current density for AHC-*600*, AHC-*700* and AHC-*800*, respectively, and remained 156, 159, and 157 F/g at 10 A/g current density, respectively.

As shown in Figure 6e, capacitance values decreased with increasing current density. Taking the capacitance value obtained at 0.5 A/g as reference, the capacitance retention for AHC-*600* at 20 A/g was remarkably high, with a value of 83% (Figure S6). This indicated that the higher content of N-species could play a key role in the capacitance performance, probably due to the occurrence of pseudo-capacitance.[16] Capacitance retention for AHC-*800* at 20 A/g was also high, with a value of 80%, owing to its relative large pore size and good electrical conductivity, which can partially promote electrolyte ions diffusion at high current densities.[1] Furthermore, the energy density and power density of all the supercapacitors were calculated from equations (2) and (3), and results were summarized in Figure 6f in the form of Ragone plots. The AHC-*700* based supercapacitor delivered high energy density of 10.6 W h/ kg at 0.1 A/g, and the energy density only decreased to 7.1 W h/ kg at current densities of 10 A/g (Figure 6f), which is comparable to that of some recently reported biomass-derived high surface area carbons.[45]

Electrochemical impedance spectroscopy (EIS) was used to evaluate the transport process of ions in the AHC-*y* N-doped carbon electrodes. Nyquist plots for all three supercapacitors exhibited a semicircle in the high- frequency region representing the bulk reaction impedance, and a straight line in the low-frequency region, typical of the capacitive behaviour of electrode (Figure 7a). In general, the smaller size of semicircle implies faster ions transfer rate with low charge-transfer resistance and the larger slope of straight lines implies the closer to an ideal capacitor and better pore accessibility.[3,5] All the AHC-*y* based supercapacitors presented tilt straight lines in low-frequency region, implying a collaborative nature of electric double layer capacitor and pseudo-capacitor.[32,45] AHC-*700* and AHC-*800* showed nearly no semicircle, in comparison to AHC-*600* that presented almost a complete semicircle. This can be partially understood if we suppose that AHC-*700* and AHC-*800* mainly contain double layer capacities, while AHC-*600* has partial pseudo-capacities, due to its higher N-species in composition, in agreement with the CV data. Equivalent series resistances of 0.28, 0.26 and 0.19 Ω were obtained for AHC-*600*, AHC-*700* and AHC-*800* based supercapacitor, respectively. Moreover, AHC-*800* displayed a much higher slope in low-frequency region, showing the best pore accessibility with good capacitive performance, especially at high rate conditions. The cycling stability for symmetric supercapacitors at 10 A/g current density in 6 M KOH was evaluated from repeatedly charging-discharging the cell (Figure 7b, Figure S7). The coulombic efficiency for all *EP* algae-derived N-doped carbon-based supercapacitors remained close to 100% for the whole cycling stage, indicating superior rate capability. The cycling stability for AHC-*600* and AHC-*700* based supercapacitors still retains 84 and 90% initial capacitance, respectively at 10 A/g current density, even after 10000 cycles (Figure S7). Significantly, the capacitance retention of AHC-*800* based supercapacitor is the highest across the samples with a 96% retention at 10 A/g current density after 10000 cycles (Figure 7b), showing a comparable or even

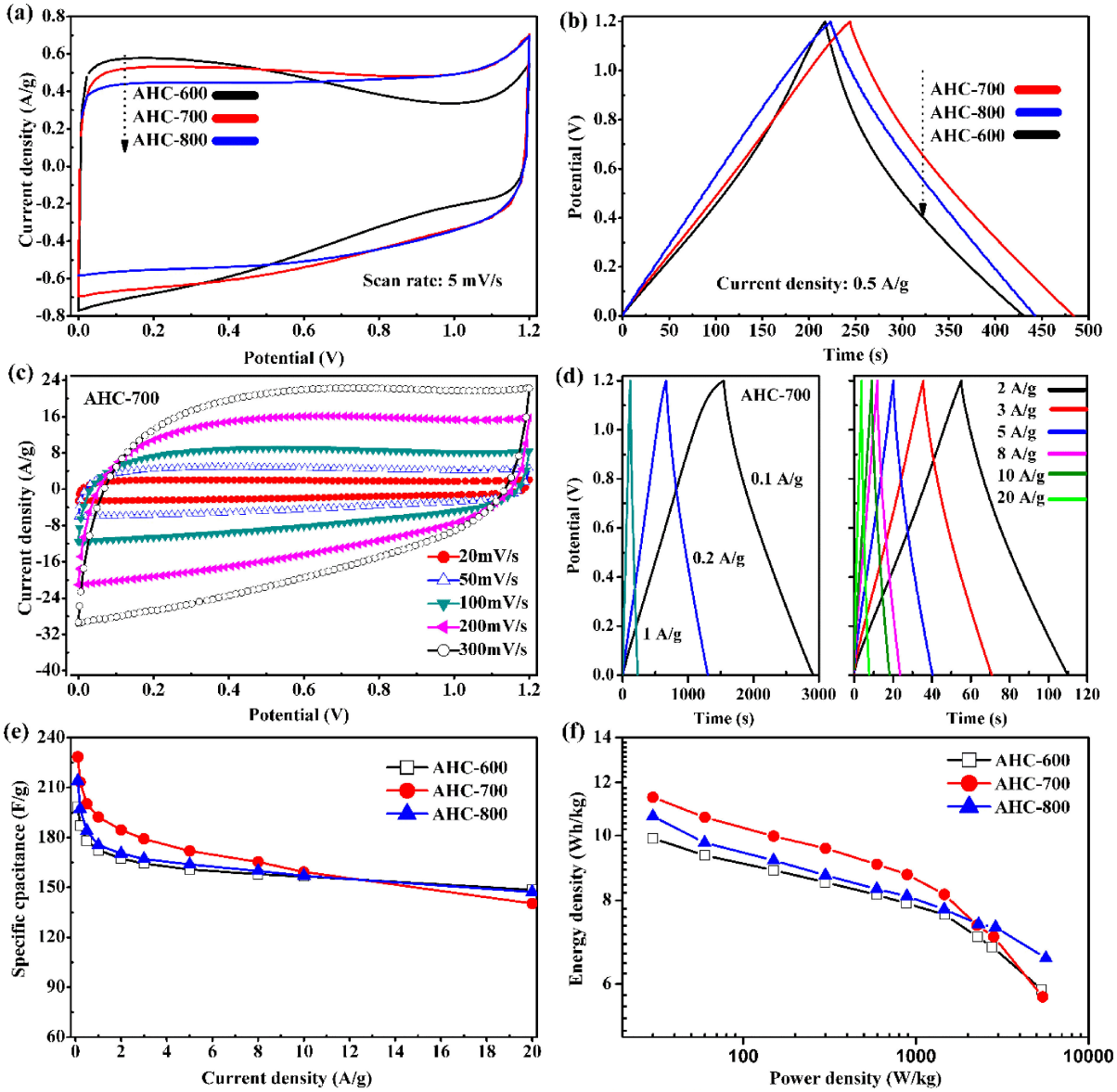

Figure 6. Electrochemical behaviour in 6 M KOH electrolyte of the AHC-*y* carbons: a), b) comparison of CV and GCD curves; c), d) CV and GCD at various conditions for AHC-*700* based supercapacitor; e) capacitance at various current densities; f) Ragone plots of energy and power density.

superior cycling performance to some other previously reported carbons from the conventional carbonization and KOH activation method using natural biomass as precursors such as *EP* algae,[33,35] bamboo[44] and wheat straw.[46] The great cycling performance of AHC-*800* is attributed to the fact that most of pores within the structure are small-sized mesopores, of 1.5 to 3.0 nm,[4,42] which can act as the ions' highways and facilitate fast diffusion into the bulk of electrodes, shortening the diffusion distance from external electrolyte to the interior surface. Another reason could be that AHC-*800* has the highest ratio of pyrrolic N in the total N-species (Figure 5), and N-species located at edges would create more active sites for better adsorption of electrolyte ions. Based on the above experiments, the synergetic effects between the existing small-sized mesopores, high-surface-areas, and N-species are indeed favourable for these *EP* algae-derived N-doped carbons with high capacitance, low resistance, and excellent cycling stability even at 10 A/g current density, making them high performance electrode materials for supercapacitors and holding great potential in future practical applications.

3. Conclusions

N-doped carbons were obtained from hydrothermal pyrolysis and KOH activation route using *EP* algae as precursors, showing high surface area of ~2000 m^2/g with N-species content of ~2.9 at.% and pores of less than 3.0 nm size, which are varied with the activation temperature. The present N-doped carbons showed high performance when tested as electrodes for supercapacitor applications, displaying 202 F/g capacitance at 0.5 A/g for AHC-700 activated at 700 °C and the capacitance

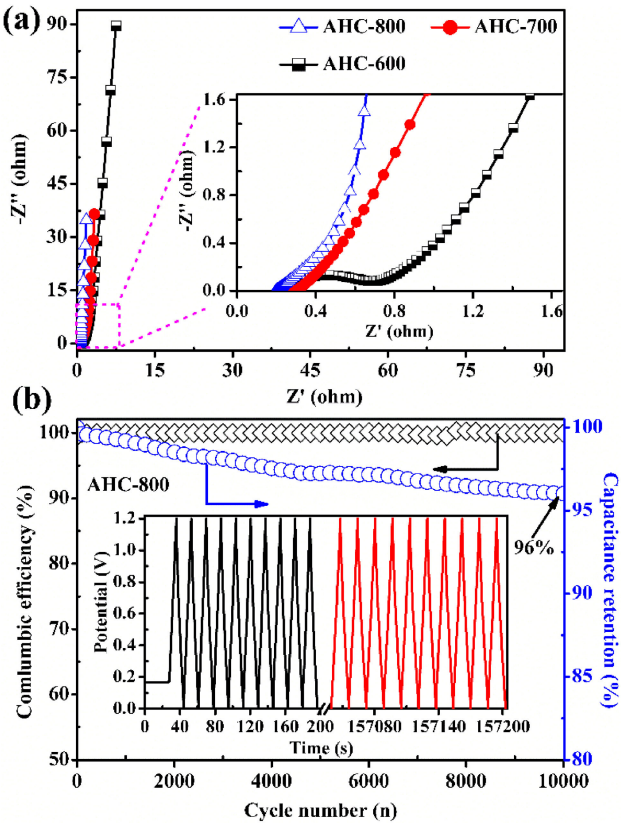

Figure 7. a) Nyquist plots for supercapacitors with AHC-*y* as electrodes; *inset*: enlarged high-frequency region. b) Cycling stability for AHC-*800* based supercapacitor at 10 A/g in 6 M KOH electrolytes and inset is the first 10 cycles and last 10 cycles.

retention of up to 96% after 10,000 cycles for AHC-800-based supercapacitor, even at 10 A/g current density, in 6 M KOH. The present results indicated that the capacitive performance is highly dependent on balance between the surface areas, mesopores and N-loadings in the framework. The symmetric supercapacitor exhibited high energy density of 7 Wh/kg and power density of 3000 W/kg, making these *EP*-derived N-doped carbons remarkable candidates for compact energy storage devices. The conversion of algae biomass into N-doped carbon shows promising perspective for supercapacitor technology, providing highly environmental benignity and cost-effectiveness in potential large-scale production.

Experimental Section

Preparation of N-Doped Activated Carbons from *EP* Algae

Fresh *EP* was collected from the coast of Qingdao, China, in July 2016, followed by the removal of impurities and subsequently freeze-dried, as described elsewhere.[30,33] Typically, 2.5 g freeze-dried *EP* were dispersed in 70 mL distilled water and hydrothermally treated in a 100 mL autoclave at 180 °C for 24 h.[29] The black solid was collected by filtration and dried at 120 °C for 24 h, followed by further carbonization at 450 °C for 2 h under N_2 (g) atmosphere, that led to the formation of biochar. This biochar was then chemically activated with KOH (KOH/char weight ratio: 2/1) at temperatures in the range of 600–800 °C at 2 °C/min for 1 h. Finally, the obtained N-doped carbon was washed with 2 M HCl at 60 °C for 3 h and distilled water and dried at 120 °C overnight. The yields varied between 13 and 25% depending on the activation temperature. The samples were labelled as AHC-*y*, where *'y'* refers to activation temperature. This will be the nomenclature used in this manuscript.

Materials Characterization

Thermogravimetric analysis (TGA) of dried *EP* macroalgae and biochars was conducted at 10 °C/min up to 800 °C under N_2 (g) atmosphere (TGA/1600HT, METTLER TOLEDO). The structure and morphology were studied by X-ray diffraction (XRD, D8 Advance diffractometer), Raman spectroscopy (Renishaw-inVia spectrometer), scanning electron microscopy (SEM, JEOL JSM6610LV), and transmission electron microscopy (TEM, Tecnai G2 F20). The surface-doping chemistry was evaluated by X-ray photoelectron spectroscopy (XPS, ESCALAB 250Xi). N_2 isotherms were conducted using a volumetric adsorption analyzer (Micromeritics TriStar II 3020) after evacuation for 6 h at 200 °C. Brunauer-Emmett-Teller (BET) method was used to calculate the surface area. Total pore volume was determined from adsorbed amount of N_2 at P/P_0 of 0.99. Pore size distribution (PSD) curves were calculated based on the nonlocal density functional theory (NLDFT) from adsorption branch of N_2 isotherms, assuming slit-pore geometry.

Electrochemical Evaluation

Electrodes were processed by preparing a slurry consisting of N-doped carbons (AHC-*y*), poly(tetrafluoroethylene), and carbon super-P in ethanol in the ratio (AHC-*y*: PFTE: carbon super-P = 80 wt%: 10 wt% in 60 wt% suspension in H_2O: 10 wt%). The slurry was pressed on a Ni foam (*d*.10 mm) that served as current collector. After drying it overnight at 90 °C in a vacuum oven, the electrode was pressed under 10 MPa pressure to increase contact between current collector and active material and minimize losses. The final loading of active material was 4.5 mg. The symmetric supercapacitors were assembled by separating two of the prepared electrodes using a glassy fiber separator (Waterman, GF/B). Cyclic voltammetry (CV) was conducted between 0 and 1.2 V at various scan rates ranging from 5 to 300 mV/s. Galvanostatic charge-discharge (GCD) was performed at various current densities ranging from 0.1 to 20 A/g. Electrochemical impedance spectroscopy (EIS) was conducted in frequencies ranging from 10 mHz to 100 kHz with an amplitude of 5 mV. All electrochemical experiments were carried out in 6 M KOH electrolyte using a potentiostat (VSP, BioLogic Science Instruments). The specific capacitance (C, F/g) of electrode for symmetric supercapacitor, and the corresponding energy density (E, Wh/kg) and power density (P, W/kg) for symmetric supercapacitor were calculated from discharge curves based on the following equations [Eq. (1)–(3)]:[3,35]

$$C = 2\frac{I \cdot \Delta t}{m \cdot \Delta V} \quad (1)$$

$$E = \frac{C \cdot \Delta V^2}{2*4*3.6} \quad (2)$$

$$P = 3600\frac{E}{\Delta t} \quad (3)$$

where I (A) is the constant charge-discharge current, m (g) is the mass of active material per electrode, Δt (s) is the discharging time,

and ΔV (V) is potential range in discharging process excluding the voltage drops (IR) value.

Acknowledgements

We thank supports from National Nature Science Foundation of China (21506184) and CSC. Authors also give thanks to Graduate Innovation (CX2017B335) and Educational Department (16C1536) of Hunan Province, and Hunan 2011 Collaborative Innovation Center of Chemical Engineering with Environmental Benignity and Effective Resource Utilization. A. Belen Jorge thanks the UK Engineering Physical Research Council and her EPSRC First Grant EP/P031323/1.

Conflict of Interest

The authors declare no conflict of interest.

Keywords: Biomass · Hydrothermal carbonization · N-doped carbon · Electrode · Supercapacitor

[1] H. Wei, H. Chen, N. Fu, J. Chen, G. Lan, W. Qian, Y. Liu, H. Lin, S. Han, *Electrochim. Acta* **2017**, *231*, 403–411.
[2] M. Sevilla, G. A. Ferrero, A. B. Fuertes, *Carbon* **2017**, *114*, 50–58.
[3] W. Yu, H. Wang, S. Liu, N. Mao, X. Liu, J. Shi, W. Liu, S. Chen, X. Wang, *J. Mater. Chem. A* **2016**, *4*, 5973–5983.
[4] H. Chen, D. Liu, Z. Shen, B. Bao, S. Zhao, L. Wu, *Electrochim. Acta* **2015**, *180*, 241–251.
[5] K. Wang, M. Xu, Y. Gu, Q. H. Fan, *J. Power Sources* **2016**, *332*, 180–186.
[6] C. Long, J. Zhuang, Y. Xiao, M. Zheng, H. Hu, H. Dong, B. Lei, H. Zhang, Y. Liu, *J. Power Sources* **2016**, *310*, 145–153.
[7] D. Zhu, H. Li, Y. Su, M. Jiang, *J. Solid State Electrochem.* **2017**, *21*, 2037–2045.
[8] Y. Pan, M. Xue, M. Chen, Q. Fang, L. Zhu, V. Valtchev, S. Qiu, *Inorg. Chem. Front.* **2016**, *3*, 1112–1118.
[9] D. Li, J. Zhou, Z. Zhang, L. Li, Y. Tian, Y. Lu, Y. Qiao, J. Li, L. Wen, *Carbon*, **2017**, *114*, 496–503.
[10] S. Xian, F. Xu, Z. Zhao, Y. Li, Z. Li, Q. Xia, J. Xiao, H. Wang, *AIChE J.* **2016**, *62*, 3730–3738.
[11] J. W. F. To, J. He, J. Mei, R. Haghpanah, Z. Chen, T. Kurosawa, S. Chen, W.-G. Bae, L. Pan, J. B. H. Tok, J. Wilcox, Z. Bao, *J. Am. Chem. Soc.* **2016**, *138*, 1001–1009.
[12] M. Sevilla, W. Gu, C. Falco, M. M. Titirici, A. B. Fuertes, G. Yushin, *J. Power Sources* **2014**, *267*, 26–32.
[13] M. Sevilla, C. Falco, M.-M. Titirici, A. B. Fuertes, *RSC Adv.* **2012**, *2*, 12792–12797.
[14] B. Hu, K. Wang, L. Wu, S.-H. Yu, M. Antonietti, M.-M. Titirici, *Adv. Mater.* **2010**, *22*, 813–828.
[15] S. M. Heilmann, H. T. Davis, L. R. Jader, P. A. Lefebvre, M. J. Sadowsky, F. J. Schendel, M. G. von Keitz, K. J. Valentas, *Biomass Bioenergy*, **2010**, *34*, 875–882.
[16] B. Zhu, B. Liu, C. Qu, H. Zhang, W. Guo, Z. Liang, F. Chen, R. Zou, *J. Mater. Chem. A*, **2018**, *6*, 1523–1530.
[17] M. Sevilla, A. B. Fuertes, *Energy Environ. Sci.* **2011**, *4*, 1765–1771.
[18] W. Tian, Q. Gao, Y. Tan, K. Yang, L. Zhu, C. Yang, H. Zhang, *J. Mater. Chem. A* **2015**, *3*, 5656–5664.
[19] D. I. Abouelamaiem, G. He, I. Parkin, T. P. Neville, A. B. Jorge, S. Ji, R. Wang, M. M. Titirici, P. R. Shearing, D. J. L. Brett, *Sustain. Energy Fuel* **2018**, DOI: 10.1039/C7SE00519A.
[20] A. Elmouwahidi, J. Castelo-Quibén, J. F. Vivo-Vilches, A. F. Pérez-Cadenas, F. J. Maldonado-Hódar, F. Carrasco-Marín, *Chem. Eng. J.* **2018**, *334*, 1835–1841.
[21] S. Herou, P. Schlee, A. B. Jorge, M. M. Titirici, *Curr. Opin. Green Sustain. Chem.* **2018**, *9*, 18–24.
[22] X. Zhou, F. Chen, T. Bai, B. Long, Q. Liao, Y. Ren, J. Yang, *Green Chem.* **2016**, *18*, 2078–2088.
[23] K. Wang, Y. Cao, X. Wang, Q. Fan, W. Gibbons, T. Johnson, B. Luo, Z. Gu, *Energy* **2016**, *94*, 666–671.
[24] H. Luo, C. C. Zhu, Z. C. Tan, L. W. Bao, J. J. Wang, G. Miao, L. Z. Kong, Y. H. Sun, *RSC Adv.* **2016**, *6*, 38724–38730.
[25] C. Falco, M. Sevilla, R. J. White, R. Rothe, M.-M. Titirici, *ChemSusChem* **2012**, *5*, 1834–1840.
[26] E. Raymundo-Piñero, M. Cadek, F. Béguin, *Adv. Funct. Mater.* **2009**, *19*, 1032–1039.
[27] M. Y. Song, H. Y. Park, D.-S. Yang, D. Bhattacharjya, J.-S. Yu, *ChemSusChem*, **2014**, *7*, 1755–1763.
[28] Q. Xu, Q. Qian, A. Quek, N. Ai, G. Zeng, J. Wang, *ACS Sustainable Chem. Eng.* **2013**, *1*, 1092–1101.
[29] Z. Zhang, K. Wang, J. D. Atkinson, X. Yan, X. Li, M. J. Rood, Z. Yan, *J. Hazard. Mater.* **2012**, *229–230*, 183–191.
[30] Z. Tian, Y. Qiu, J. Zhou, X. Zhao, J. Cai, *Mater. Lett.* **2016**, *180*, 162–165.
[31] D. Zhou, L. Zhang, S. Zhang, H. Fu, J. Chen, *Energy Fuels* **2010**, *24*, 4054–4061.
[32] Z. Tian, M. Xiang, J. Zhou, L. Hu, J. Cai, *Electrochim. Acta* **2016**, *211*, 225–233.
[33] X. Wu, Z. Tian, L. Hu, S. Huang, J. Cai, *RSC Adv.* **2017**, *7*, 32795–32805.
[34] X. Gao, W. Xing, J. Zhou, G. Wang, S. Zhuo, Z. Liu, Q. Xue, Z. Yan, *Electrochim. Acta* **2014**, *133*, 459–466.
[35] Y. Gao, W. Zhang, Q. Yue, B. Gao, Y. Sun, J. Kong, P. Zhao, *J. Power Sources* **2014**, *270*, 403–410.
[36] M. Wu, P. Li, Y. Li, J. Liu, Y. Wang, *RSC Adv.* **2015**, *5*, 16575–16581.
[37] X. Liu, H. Wang, Y. Cui, X. Xu, H. Zhang, G. Lu, J. Shi, W. Liu, S. Chen, X. Wang, *J. Mater. Sci.* **2018**, 53, 6763–6773.
[38] Y. Li, D. Li, Y. Rao, X. Zhao, M. Wu, *Carbon* **2016**, *105*, 454–462.
[39] J. Cai, J. Qi, C. Yang, X. Zhao, *ACS Appl. Mater. Interfaces* **2014**, *6*, 3703–3711.
[40] F. Bonhomme, J. C. Lassègues, L. Servant, *J. Electrochem. Soc.* **2001**, *148*, E450-E458.
[41] S. Devaraj, H. Y. Liu, P. Balaya, *J. Mater. Chem. A* **2014**, *2*, 4276–4281.
[42] L. Guo, X. Wang, Y. Wang, *Chem. Eng. J.* **2017**, *313*, 1295–1301.
[43] V. Selvamani, R. Ravikumar, V. Suryanarayanan, D. Velayutham, S. Gopukumar, *Electrochim. Acta* **2016**, *190*, 337–345.
[44] Y. Gong, D. Li, C. Luo, Q. Fu, C. Pan, *Green Chem.* **2017**, *19*, 4132–4140.
[45] G. Zhu, L. Ma, H. Lv, Y. Hu, T. Chen, R. Chen, J. Liang, X. Wang, Y. Wang, C. Yan, Z. Tie, Z. Jin, J. Liu, *Nanoscale* **2017**, *9*, 1237–1243.
[46] S. Zhang, K. Tian, B.-H. Cheng, H. Jiang, *ACS Sustainable Chem. Eng.* **2017**, *5*, 6682–6691.

Manuscript received: May 7, 2018
Accepted Article published: June 19, 2018
Version of record online: July 2, 2018